Emulating Nuclear Emissions with a Pulsed Laser

Benjamin J. Hockman, Jianxin Sun and Herbert G. Tanner

***Abstract*—The paper presents an approach to emulate the Poisson process observed by a sensor when subject to low levels of radiation, motivated by the problem of detecting a weak source in the presence of background radiation. We construct a physical emulation of this process to serve as a means of experimentation for various detection models involving mobile sensor networks. A pulsing laser emulates the nuclear emission, and a rotating mirror deflects the pulses in a random direction. The degree to which the proposed emulation process matches actual radiation measurement results is assessed experimentally, and the utility of the device is demonstrated and compared against conventional methods in a simple detection scenario.**

***Note to Practitioners*—This paper describes the design principles of a pulsed laser apparatus that emulates the emission of radioactivity. The device allows one to experiment with methods for radiation detection and measurement without the need to handle and store potentially hazardous radioactive material. From the perspective of a user that counts events (rather than in terms of the physical signal expressing the energy deposited on the sensor) the experimental apparatus described here behaves very similarly to a pair of radioactive source and Geiger counter.**

***Index Terms*—Poisson process, radiation detection, sequential testing.**

I. Introduction

This paper presents a mechanism that physically emulates nuclear emission, for the purpose of analysis and testing of algorithms for low-level radiation detection, without the need for handling radioactive material. The physics of gamma ray emissions is very similar in nature to that of radiation at other frequencies, but it is the intensity and timescale of these emissions that make them unique from an observational standpoint. Visible light, for example, is actually a stream of discrete photons and electromagnetic waves, but the intensity is typically large enough that they can be well approximated by an averaged intensity or flux. However, if the lights are dimmed low enough, the "average photon flux" becomes difficult to estimate because the separation between photons is large. This is the region that is most prevalent when dealing with low level gamma radiation. As an analogy, think of visible light as a steady flow of water through a hose and gamma radiation as a slowly dripping faucet. We would need different measurement techniques to estimate the flow rate of each.

The discrete process of gamma ray arrivals at a Geiger counter closely conforms to Poisson statistics. Typically, a Poisson process is characterized by its intensity (λ)—or average number of events per unit time. This particular stochastic process is defined by the exponential probability density function (PDF) for the time between events with mean $1/\lambda$ given by

$$P(x;\lambda) = \lambda e^{-\lambda x}, \qquad x \geq 0 \ . \tag{1}$$

It turns out that Poisson processes are ubiquitous in modeling natural phenomena and are by no means restricted to describing radioactive decay. Generally, most continuous-time counting processes with independently occurring events can be well modeled with this process; some examples include the number of points scored during a basketball game, hits on a web page, and the number of raindrops falling within a specified area [1].

Now consider the following regime: we have two radiation sources generating independent Poisson emissions in parallel with intensities λ_1 and λ_2. At t_0, λ_1 is turned on and at $t_1 = 1$ s, λ_2 is turned on. They both emit gamma rays, so a nearby sensor can only pick the sum of both emissions $\lambda_1 + \lambda_2$. Now suppose that this sensor—with no knowledge of the binary states of each source—needs to decide between two hypotheses H_0 and H_1 at a given time T after the second source is turned on, where (i) H_0: only λ_1 is turned on, and (ii) H_1: both λ_1 and λ_2 are turned on. This is an instance of an inverse problem, posed as a binary hypothesis decision problem.

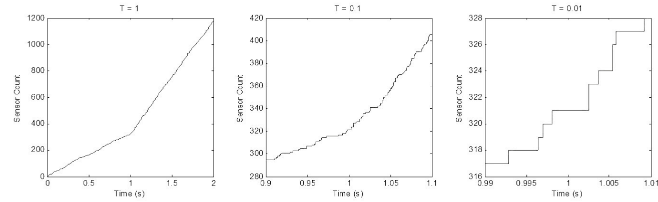

Fig. 1: A simulation of Poisson process with $\lambda_1 = 300$ Hz at $t > 0$ and $\lambda_2 = 600$ Hz at $t > 1$.

An example of what this sensor might observe in this *fixed interval detection paradigm* is illustrated in Fig. 1 for three values of T. These three plots illustrate why the ability of a sensor to make a decision between H_0 and H_1 is highly dependent on the observation interval T. The naked eye can tell that there is clearly a change in count rate for $T = 1$, but it becomes less obvious at $T = 0.1$ and almost indistinguishable at $T = 0.01$. Similarly, any decision made between H_0 and H_1 exhibits a confidence level roughly proportional to T. Indeed, the fundamental goal of the binary detection problem is to make a decision between the two hypotheses as quick as possible while minimizing the chances of error.

This scenario is common in the problem of timely detection of a radiation source. There, $\lambda_1 \equiv \beta$ corresponds to the activity rate of background radiation that is confounding the source to be detected, the activity of which is expressed by $\lambda_2 \equiv R$. In general, the background intensity β is non-homogeneous and position dependent (i.e. $\beta = \beta(\vec{X}, t),\ \vec{X} \in \mathbb{R}^3$), but for most cases we can assume β to vary only with position, and its spatial distribution can either be assumed known or it can be measured [2].

The radiation due to the source is also non-homogeneous in nature. It is generally assumed to be proportional to the square of the distance of the sensor from the source (i.e. $R \propto 1/r^2$)[1] [3]. The relationship reflects the dispersion of gamma ray density from a point source in $\mathbb{R}^3$, and suggests that an approach to detection of low-level radiation is not necessarily specific to weak sources, but is also applicable to cases of more active sources, which may either be shielded or sufficiently far away from the sensor. In fact, many important applications of low-level detection such as mobile searches for dirty bombs or passive surveillance screening for hazardous radioactive materials [4] deal with shielded sources observed at a distance over a short period of time, making them difficult to detect.

In this paper, we describe the design, fabrication and validation of an apparatus that emulates the mechanism of nuclear decay and radiation measurement without using fissile material. We demonstrate its use for detection in experiments, and compare the results with those obtained by a Geiger counter. The solution proposed consists of a laser that produces short pulses of light to mimic the emission of discrete gamma rays, coupled with a reconfigurable mirror used to scatter the laser beams in random directions, and a photo-detector in the role of the radiation counter. The laser pulses are modulated by a computer controlled relay switch that determines the source intensity

[1]The relationship suggests that R increases unboundedly as $r \to 0$, but is valid under the assumption that the sensor maintains a minimum distance $\delta > 0$ from the source.

The authors are with the Department of Mechanical Engineering, University of Delaware, Newark DE 19716.

by varying the mean frequency of pulses. Our goal is to meaningfully capture the statistics of nuclear measurement, and faithfully replicate the dependence of the observation statistics on the distance between sensor and source, in a framework where we have absolute control over the parameters of the emulated physical process.

A. Related Work

The mathematics of decision theory has grown significantly over the past few decades. Some of the work done in the detection of signals that follow Poisson statistics can be attributed to its application in optical communications. It turns out that an avalanche photodiode (APD) attempting to pick up a modulated optical signal transmitted through a noisy medium often faces the same type of detection regime as a radiation sensor attempting to pick out a weak signal from background noise [5]–[9]. The roots of sequential hypothesis testing were established in the early 1950s with Wald's sequential probability ratio test (SPRT) [10]. The test provides a time-optimal strategy for hypothesis testing of continuous processes such as the Poisson process. However, applying this method to different applications often requires more specific formulations, with adapted time-optimal solutions. For example, a Bayesian inference solution for the decision between two intensity values (λ_1 or $\lambda_1 + \lambda_2$) under the regime outlined in Section I is found in [11]. An alternative formulation for this binary decision problem is the Neyman-Pearson test [12]. A formal solution to the Neyman-Pearson formulation can be adapted from a Bayesian approach and can be found in [13] (see also [3], [14] for network variants). There are also different ways to define the detection specifications within each hypothesis formulation. For the case of radiation detection, we can think of a case where a sensor is given a finite time interval in which it must make a decision (fixed-interval test [15], [16]), or another case in which the sensor will only make a decision if its confidence level exceeds a threshold [17].

For the general problem of detecting a mobile source that traverses a restricted area of observation in 2D, we know how to interpret the data gathered from a single static sensor, and even how to fuse data from multiple sensors [3], but the problem of detection with mobile sensor networks is still open. Introducing mobility into sensor networks may significantly enhance their detection capabilities. It also raises many new questions such as how to optimally configure sensor positions and plan trajectories to gather a maximum amount of information or how to fuse data from a network of stationary and mobile sensors. These are the questions that we are beginning to ask in order to advance the frontier of understanding in radiation detection.

B. Scope and Organization

There is a need for an experimental platform on which theory and algorithms for radiation detection can be tested without having to handle hazardous material. To this end, we suggest to controllably emulate the physics of radiation emission in a way such that sensor observations mimic the response of a Geiger counter in the presence of radiation. The ability to precisely control various physical parameters—from both an emission and detection standpoint—is the essence of why we desire this emulation. Aside from providing feedback on the effectiveness of our detection models, the data gathered from this emulation experiment offer insight into how our models can be improved, since a number of different problem parameters are easily tunable, from the source activity to the size and sensitivity of the sensor. The remainder of this paper discusses how this is achieved. Section II outlines the problem scope more thoroughly and breaks down the problem into smaller sub-problems to be addressed. Section III describes exactly how the emulation works, how it meets the design specifications, and its various capabilities and limitations. Section IV outlines the experimental results that verify the system performance, and the paper concludes with Section V.

II. Problem Statement

A Poisson process is a continuous-time counting process, where $\{N(t),\ t \geq 0\}$ denotes the number of events—in our case, gamma rays—that are observed. The process has the following properties:

Zero at initial time $N(0) = 0$.

Independent intervals: the number of events in disjoint intervals is mutually independent. That is if $t_1 < t_2 < t_3 < t_4$, then $N_A(t_2 - t_1)$ and $N_A(t_4 - t_3)$ are independent for a given Poisson process.

Stationary increments: the probability distribution of events in any sub-interval (τ) is only dependent of the length of the interval $N \equiv N(|\tau|)$.

No counted events occur simultaneously.

The probability distribution of $N(t)$ is a Poisson distribution

$$\mathbf{P}(N(t) = k) = \frac{m(t)^k}{k!} e^{-m(t)}, \text{ where } m(t) = \int_0^t \lambda(u)\, \mathrm{d}x \ .$$

The probability of time between events is exponentially distributed given by (1).

The two Poisson processes we deal with in detection theory are defined as $\beta \equiv \beta(\vec{X})$, where $\vec{X} \in \mathbb{R}^3$, and

$$R_i(r,t) \triangleq f(r_i)\lambda_i(t), \quad f(r_i) \triangleq \frac{1}{1 + (\frac{r_i}{K_{1/2}})^2} \tag{2}$$

Here, the background intensity β is only a function of spatial position, and is known to the sensor. Variable R_i is the intensity observed by the sensor from source i and is factored into functions of position and time.[2] Variable r_i is the distance of the sensor from source i, and $K_{1/2}$ is the distance at which its intensity falls off to half its maximum value λ_i. This form of $f(r_i)$, suggested in [18], incorporates the $1/r^2$ falloff but does not blow up at $r_i \to 0$.

In our emulation we would like to have control over the following variables: (a) Intensity and distribution of background Poisson process β; (b) Total source emission as a function of time $\lambda_i(t)$; (c) Half-intensity distance is controlled by the area of the sensor $K_{1/2}$; (d) Radial distance between the source and sensor r_i. In designing a device that emulates such a process, we attempt to isolate these variables as much as possible.

III. Technical Approach

A. Challenges

Putting a radioactive source in the vicinity of a Geiger counter, and measuring the response directly, has limitations which may render it impractical in some cases. For instance, the intensities of radiation sources are not easily controlled because they depend on material composition, while background levels are environment-dependent. Furthermore, low-level sources that are not hazardous have a small detectable range, which limits the physical scale of potential experiments. For example, a weakly radioactive Uranium oxide bead is only detectable to a distance of approximately 4cm. This range is not large enough to incorporate sensor mobility on robotic platforms.

[2] We will often take $\lambda_i(t)$ to be constant, but this is the more general non-homogeneous representation.

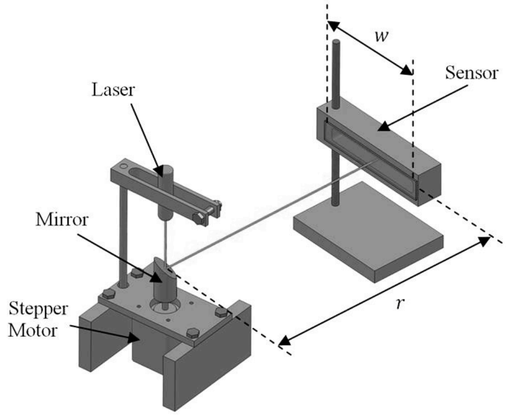

Fig. 2: Solidworks™ rendering of the experimental setup: r is the distance between sensor and mirror; w is the detectable width of sensor.

B. Generating the Poisson Process

The solution proposed is to physically emulate the gamma-ray emission process using pulses from a controlled laser light source. The apparatus designed to implement this solution produces short pulses of light. These pulses are modulated by a computer controlled relay switch that determines the source intensity by varying the mean frequency of pulses. The laser beam is then reflected at a 90° angle by a mirror. This mirror is fixed to the shaft of a stepper motor which rotates randomly. As a result, each pulse of the laser is redirected in a random planar direction to create a 360° emission spectrum. Finally, a light sensor (or array of sensors) is positioned in the plane of emission such that it picks up only a fraction of pulses. Figure 2 depicts a SolidWorks™ rendering of the device. The binary states of the laser are controlled by software, which uses the desired source intensity λ as an input (in Hz or pulses/sec), and generates the Poisson process by creating a random array of time between pulses that is exponentially distributed with mean $1/\lambda$.

C. Pulse Detection

The light sensor positioned in the emission plane of the laser reports high light intensity when the laser beam is incident on it, and ambient levels at all other times. The capabilities of the sensor are important to the type of detection strategies it can handle. In our case, the sensor is not a counter, but it merely returns the light intensity value when interrogated by software. This exposes a challenge, because if the sensor has no prior knowledge of when the laser will flash, it can only sample finite instants in time when checking for an event occurrence. We address this issue by controlling the laser and sensor through the same software process, in a way that the sensor only checks for a light pulse if the laser is told to pulse. In this manner, we can ensure that the detector is "on" when the laser sends a pulse.

D. Composing Background and Source Emissions

The apparatus we have constructed (see Fig. 4) has only one emitting source. However there are a few ways in which we can effectively generate two parallel Poisson processes (β and λ). For the most restricted case of a fixed sensor and source (i.e. $\frac{dr}{dt} = 0$), we can have the laser generate both β and λ by superposing their intensities such that the total intensity is given by $\Lambda(t) = \lambda(t) + \beta$. For a more general case in which sensors are mobile (or they are static but the source is moving) we cannot generate β with the laser, because its intensity would scale with $1/r$, just as the source's. The most direct way to create the background emission would be to simulate the background signal and send it directly to the detector. This can be done without using the light sensor, as long as the detector cannot tell if an event is coming from β or from λ. Knowing the position of the sensor at a given time (via a priori knowledge or sensory input), a radiation map $\beta(\vec{X})$ can also be incorporated [2].

E. Distance of Sensor

Recall that the intensity of radiation incident on a sensor exhibits a $1/r^2$ falloff given by (2). For simplicity, our emulation process is restricted to emissions in $\mathbb{R}^2$, so the falloff is instead proportional to $1/r$. This is due to the fact that in $\mathbb{R}^3$ the sensor area creates a solid angle as viewed by the source (measured in radians squared), whereas a sensor in $\mathbb{R}^2$ creates a standard angle to the source. Since the solid angle is given by $\Omega \approx \alpha^2$ and $\alpha \propto \frac{1}{r}$ $(\alpha \ll 1)$, it follows that the fractional incidence in $\mathbb{R}^3$ is proportional to $1/r^2$, but in $\mathbb{R}^2$ it is only proportional to $1/r$. Keeping this in mind, one can extrapolate the effects observed in $\mathbb{R}^2$ into the $\mathbb{R}^3$ domain.

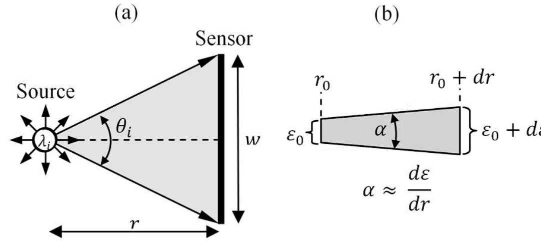

Fig. 3: (a) Schematic of laser emission in $\mathbb{R}^2$, (b) element of laser beam scattering

Let us examine more closely how well this relation holds. Figure 3 a shows a simplified schematic of the laser and sensor with a view orthogonal to the emission plane. At close range, the fractional incidence function $f(r)$ is given by $f(r) = \frac{1}{\pi}\tan^{-1}\left(\frac{w}{2r}\right)$. However, as $\frac{w}{r} \rightarrow 0$, we have that $\lim_{w/r\rightarrow 0} f(r) = \frac{w}{2\pi r}$. Practically, this approximation is accurate to within 1% when $w < 3r$. This relationship also relies on two assumptions concerning the laser beam (refer to Fig. 3b): (i) the width of the laser beam is significantly smaller than the sensor width, i.e., $\varepsilon \ll w$, and (ii) the scattering angle of the beam is significantly less than the incidence angle, i.e., $\alpha \ll \theta_i$. In our case, both assumptions are valid. For 1) we have that for practical ranges ($r < 10$ ft) it is $\varepsilon_{max} \approx 5$ mm, $w_{max} \approx 100$ mm; while for 2) it is true that for this combination of laser and mirror, $\alpha \approx 10^{-3}$ rad, $\theta_{i_{min}} \approx 0.02$ rad (at $r = 10$ ft). In summary, the sensor incidence will be proportional to $1/r$ if $3 < \frac{r}{w} < 100$ and $w > 2$ inches. These requirements may be relaxed if a more focused laser is used.

F. Scaling: The Equivalent Sensor

The equation that models how perceived intensity at the sensor's end scales with distance from the source,[3]

$$R_i = \frac{\chi\alpha}{1 + r_i} \tag{3}$$

reveals possibilities for emulating a wide range of detection scenarios by varying the apparatus design parameters. For example, a milligram of Potassium (present in bananas) would register roughly $\alpha = 0.031$ counts per second (almost two per minute) at point-blank range, whereas a milligram of Caesium-136 would theoretically register more than $\alpha = 3 \times 10^9$ counts per second. Shielding such quantities

[3]In 3D, the r_i term in the denominator is squared.

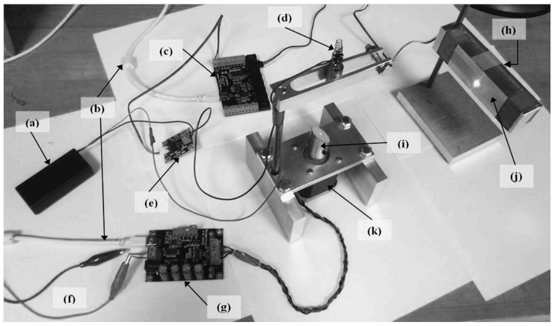

Fig. 4: Physical setup of emulation: (a) battery pack (b) USB cables to computer (c) Phidget Interface Kit (d) laser (e) solid state relay switch (f) wires to power supply (g) stepper controller (h) light sensor (i) mirror (j) enclosed sensor housing (k) stepper motor.

can drop their perceived emission rates by orders of magnitude. Despite how much different in scale these activities are, for appropriate ranges between source and detector, they may still be emulated using the same laser source by adjusting the characteristic surface constant χ and range r_i in the apparatus, so that the perceived activities (3) at sensor i in emulation and real-life cases, match.

Moreover, the proposed scheme is capable of emulating a *collection* of detectors distributed on the *plane*—in $\mathbb{R}^3$, the scaling is different, but the same principles apply. For clarity of presentation, assume n identical[4] detectors of characteristic surface constant χ, positioned at ranges $r_1, \ldots, r_n$ from a source of activity α. This distributed collection of sensors register counts at a rate equivalent to a single, bigger, "equivalent" sensor at a distance r_0, which has characteristic surface constant χ_0. If r_0 is given, then χ_0 can be determined from (3) as follows.

Virtually relocate sensor i from its current range r_i to the desired equivalent sensor's range r_0, scaling its characteristic surface from χ to χ_i in a way that the ratio of (3) remains constant; from that relation, χ_i is determined:

$$\frac{\chi\alpha}{1+r_i} = \frac{\chi_i\alpha}{1+r_0} \implies \chi_i = \frac{\chi(1+r_0)}{1+r_i} .$$

Then the characteristic surface constant of the equivalent sensor, χ_0 is obtained by assuming that all these virtual sensors are fused together in a way that their surfaces are added up. The latter is found by computing he "equivalent" component of each sensor when it is moved from distance r_i to distance r_0:

$$\chi_0 = \sum_{i=1}^{n} \frac{\chi(1+r_0)}{1+r_i} ,$$

and a single equivalent sensor at range r_0, with that surface constant will be subject to the same measurement source photon arrival statistics as the collection of the distributed detectors.

However, the background photon arrival statistics do not scale in the same way with range. For simplicity, let us assume that background radiation is uniform over the plane. Then, the background photon arrival (Poisson) statistics at the equivalent sensor should be taken with mean

$$\beta_0 = \beta\frac{\chi_0}{\chi} = \beta\sum_{i=1}^{n}\frac{1+r_0}{1+r_i} .$$

G. Directional Randomness

Rays emitted by a high-energy nucleus are theoretically distributed uniformly around it. Our emulation device, driven by a stepper motor, can achieve finite, but adequate resolution at 6400 steps per revolution. In the device described, the stepper motor is synchronized with laser emission, so that it rotates to a (uniformly) random location immediately after each pulse. Thus, the laser emits pulses only while the mirror is stationary, but still the direction of emission remains random. This approach also allows for the possibility of imposing directional bias or non-uniformity in the emission such that $\lambda = \lambda(\theta, t)$. To generate some arbitrary (directional) intensity $\lambda(\theta, t)$, it suffices to control the stepper motor so that it rotates the mirror to random positions skewed along a particular direction.

[4] The assumption can be easily relaxed.

H. Computation Delay Errors

The time between laser pulses is specified in a vector of random samples from the exponential distribution. However, software's computational overhead induces a—roughly uniform—error and skews the Poisson process. Effectively, the computation time in each iteration, denoted $\delta\tau$, adds to the desired dwell time, resulting in an effective wait time between pulses of $\tau_{average} = \frac{1}{\lambda} + \delta\tau$, where λ is the desired intensity. The lag is determined by how computationally intensive the loop is, and includes any additional overhead imposed by reporting and logging application requirements. Since the desired value for $\tau_{average}$ is $\frac{1}{\lambda}$, a lower value of λ can practically eliminate the error that the computation lag induces. There is a lower bound, however, to how much this lag can be reduced, since it also includes the laser pulse duration which may not be under the direct control of the designer.

IV. Experimental Results

A. Emulation of Nuclear Emission

To verify that this emulation accurately models radioactive emissions, we run experiments to compare the sensor data to observations from an actual Geiger counter. We confirm that the time between counts follows the exponential distribution and that the source intensity falls off as $1/r$.

Initially, a background sample is taken from the Geiger counter over a 24 hour period—long enough to discern a stable mean intensity and robust distribution. The output from the Geiger counter is a chronological timestamp vector of gamma ray events, which is then processed to give the times between two consecutive events. The data is sorted into one second bins and normalized to fit an exponential PDF. As expected, the exponential regression is a very strong fit, with a correlation coefficient approximately equal to one (see Fig. 5).

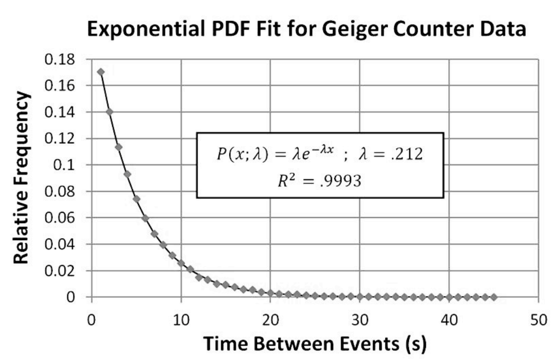

Fig. 5: A 24-hour sample of background radiation ($n \approx 20,000$) from a Geiger counter. Exponential PDF fit shows a very strong correlation.

A three-hour trial with about 6000 samples on the emulation device provides a data set that yields an exponential regression correlation coefficient of $R^2 = 0.997$ (Fig. 6). A computational lag of magnitude

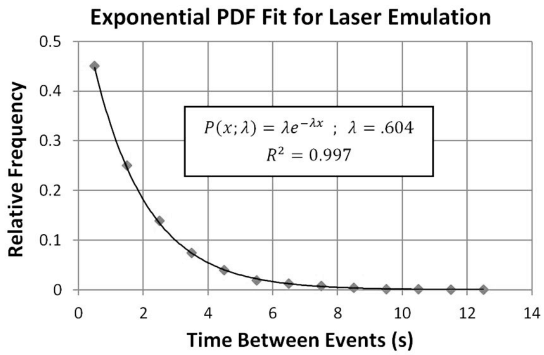

Fig. 6: A three-hour sample from device emitting Poisson background ($n \approx 6,000$). The curve is shown shifted 0.1 s left to compensate for the time lag of laser emission.

between 0.05 and 0.1 seconds is observed due to laser transmission—the time between two pulses can be no shorter than the duration of each pulse—and sensor recording. This effect would normally shift the exponential regression curve to the right, but is compensated for in the data reported in Fig. 6. The significance of this lag, in terms of skewing the observed event occurrence distribution, is roughly proportional to the mean intensity, and is is more pronounced at higher intensities. An intensity scale-back mitigation strategy can thus be effective (see Section III-H). Comparison of Figs. 5 and 6 indicates that the emulation device reproduces the Poisson process.

We now validate the range-scaling behavior. The radioactive source used in conjunction with the Geiger counter is a small bead of vaseline glass—only detectable to a distance of about 4 cm. Five separate trials are conducted within this range for about 20 minutes each. The data shown in Fig. 7 strongly suggests a $1/r^2$ relationship, with a correlation coefficient of $R^2 = 0.975$. The fit is expected to be better with larger samples. The inverse square law observed for the case of vaseline glass and Geiger counter is not surprising, because both the Geiger counter and the glass bead operate in $\mathbb{R}^3$, and especially at these small ranges, the detector surface is associated with a significant *solid angle*. The intercept of the linear regression represents the background intensity, which is consistent with the background measurements of Fig. 5.

The variable distance scenario is emulated on the device for distances ranging between 8 inches and 28 inches. The emissions generated are a superposition of a source of constant intensity plus background. The background intensity has to be adjusted on the laser side at different distances to maintain a constant intensity on the sensor side. Each trial runs for about 3 hours and all mean intensities are shown in Fig. 8. Linear regression suggests a strong relationship between mean intensity and $1/r$, and the y-intercept value reflects the expected background intensity. Recall from Section III-E that the distance fall-off for this device is proportional to $1/r$ because the emissions are restricted to a plane ($\mathbb{R}^2$).

B. Application to Detection

The goal of having such device is to extend the possible range of detecting radioactive sources in emulation. To this end, we compare a fixed-interval detection emulation scenario to the case of detecting the vaseline bead with the Geiger counter.

The standard likelihood ratio test[5] (see [12]) forms a ratio based on collected data and compares it to a preset threshold. If the likelihood ratio is above the threshold, the hypothesis supporting the presence of a source of given activity is verified; otherwise, the hypothesis

[5]Its optimality origins dating back to [19].

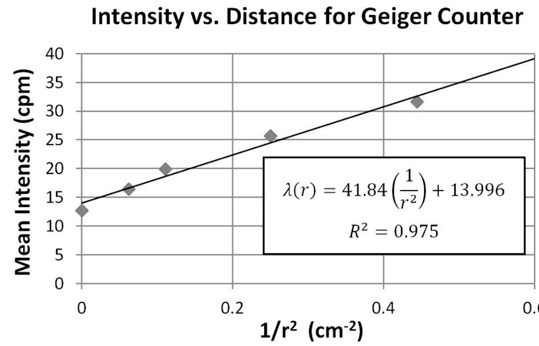

Fig. 7: Geiger counter samples in range of radioactive glass bead.

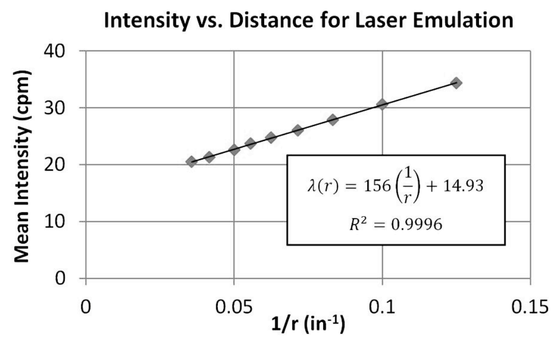

Fig. 8: Mean count frequency at sensor for distances between 8 and 28 inches from the mirror. The $1/r$ relationship is very strong.

is rejected. The likelihood ratio L_T in this fixed time-interval $[0, T]$ detection problem is [18]

$$L_T = \mathrm{e}^{-\nu T} \mu^{N_T} \ ,$$

where $\nu = \frac{\chi\alpha}{r^2}$, is the perceived source intensity at the sensor, $\mu = 1 + \frac{\nu}{\beta}$, and N_T is the total number of arrival events registered until time T, which is the time at which a decision between the two hypothesis needs to be made.

There are two types of errors that can be made in the decision process: a false alarm, and a missed detection. The two are linked, in the sense that for a given false alarm rate, there is an optimal threshold value for the ratio test for which the probability of detection is maximized [19]. In the test we run here, we treat the threshold as an independent variable, and we estimate through a large number observations for a known source, the probability of detection at different distances. A different probability-threshold curve is drawn for various ranges between light sensor and mirror (Fig. 9(a)).

To validate the laser device as an effective proxy, the curves of Fig. 9(a) should match the ones created based on detection experiments with the radioactive vaseline glass bead and the Geiger counter. The latter are placed at distances varying from 1 to 3 cm, and different 100 minute-long samples (each containing 100 decision tests) are collected at each distance. The total number of gamma rays captured by the Geiger counter is recorded for each sample. With prior knowledge of α, χ, and β, we calculate for each distance the parameters ν, μ, and the likelihood ratios. In Fig. 9(b), each curve shows the probability of detection at that distance, with the latter calculated as the ratio of successful detections over the total number of samples at that distance. As expected, the data shows an inverse relationship between detection probability and threshold. The detection probability also drops faster at longer distances. Achieving a desired detection probability, requires using increasingly smaller thresholds as the distance increases.

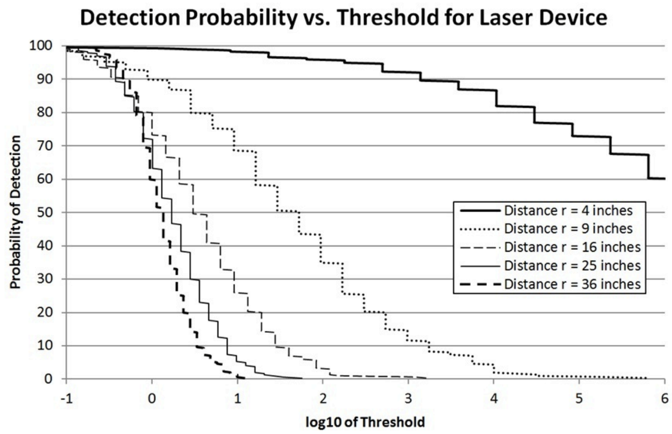

(a) Probability of detection (in percentage) vs. likelihood ratio threshold ($\log_{10}$ scale) from experiments with the laser device at distances 4, 9, 16, 25, and 36 inches.

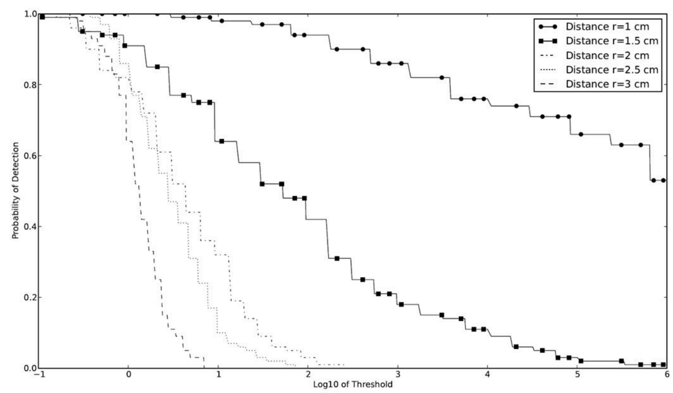

(b) Probability of detection (in absolute value) vs. likelihood ratio threshold ($\log_{10}$ scale) in bead experiment at distances 1, 1.5, 2, 2.5, and 3 cm.

Fig. 9: Comparison of detection results between emulation and experiment. Figures (a) and (b) report results at different distances because emissions from the bead are 3D while those from the laser device occur in the plane. The distances used in one test map to those in the other using the scaling relationship between the sensor solid angles in 2D and 3D: $\frac{\chi_{\text{geiger}}\,\alpha_{\text{source}}}{r^2_{\text{geiger}}} = \frac{\chi_{\text{laser}}\,\alpha_{\text{laser}}}{r_{\text{laser}}}$.

To reproduce these results with the laser device, we apply the transformations of Section III-F to match the ν and μ values of the bead–Geiger combination at five different distances. Parameters that achieve this are the ones corresponding to a 4 inch sensor scope, a pulse frequency of 2.78 Hz, and a sample time of 60 seconds. Since the laser device has a $1/r$ falloff effect, distances of 4, 9, 16, 25, and 36 inches are used with the laser device to achieve the same ν values as the 1, 1.5, 2, 2.5, and 3 cm distances with the bead and Geiger counter, respectively. The signal measured by the light sensor is added to an independent background Poisson process to produce similar μ and N_T values. The results are shown in Fig. 9(a), confirming the match in performance of the likelihood ratio test between emulation and physical experiment with the radioactive source.

V. Conclusion

This paper contributes to the analysis of the detection algorithms for weak discrete-event signals such as nuclear emissions, by proposing an experimental setup that is capable of emulating faithfully the statistics of the (Poisson) process to be detected. The experimental device consists of a laser, modulated to create short pulses of light that follow Poisson statistics, and a rotating mirror reflects each pulse in a random planar direction. The Poisson statistics and the directional randomness of the nuclear emission phenomena are captured. As a result, detection methods can equivalently be tested and validated using the proposed device, instead of the need to experiment with potentially hazardous sources of radiation. We envision the proposed setup having applications beyond the ones demonstrated in this paper, involving static sources and sensors. Specifically, we believe that the proposed methodology for emulating nuclear emissions can have applications in instances where moving signal sources are to be detected by networks of potentially mobile sensors.

References

[1] A. Papoulis, *Probability, Random Variables, and Stochastic Processes*. McGraw Hill, 1965.

[2] R. Cortez, X. Papageorgiou, H. Tanner, A. Klimenko, K. Borozdin, R. Lumia, and W. Priedhorsky, "Smart radiation sensor management; radiation search and mapping using mobile robots," *IEEE Robotics & Automation Magazine*, vol. 15, no. 3, pp. 85–93, 2008.

[3] R. J. Nemzek, J. S. Dreicer, D. C. Torney, and T. T. Warnock, "Distributed sensor networks for detection of mobile radioactive sources," *IEEE Transactions on Nuclear Science*, vol. 51, no. 4, pp. 1693–1700, 2004.

[4] R. Byrd, J. Moss, W. Priedhorsky, C. Pura, G. W. Richter, K. Saeger, W. Scarlett, S. Scott, and R. W. Jr., "Nuclear detection to prevent or defeat clandestine nuclear attack," *IEEE Sensors Journal*, vol. 5, no. 4, pp. 593–609, 2005.

[5] I. Bar-David, "Communication under the poisson regime," *IEEE Transactions on Information Theory*, vol. 15, pp. 31–37, 1969.

[6] R. Gagliardi and S. Karp, "M-ary poisson detection and optical communications," *IEEE Transactions on Communication Technology*, vol. 17, pp. 208–216, 1969.

[7] A. Lam and A. Hussain, "Performance analysis of direct-detection optical cdma communication systems with avalanche photodiodes," *IEEE Transactions on Communications*, vol. 40, pp. 810–820, 1992.

[8] M. Teich and S. Rosenberg, "Photocounting array receivers for optical communication through the lognormal atmospheric channel: optimum an dsuboptimum receiver structures," *Journal of Applied Optics*, vol. 12, pp. 2616–2623, 1973.

[9] S. Verdú, "Multiple-access channels with point-process observations: Optimum demodulation," *IEEE Transactions on Information Theory*, vol. 32, no. 5, pp. 642–651, 1986.

[10] A. Wald, "Sequential tests of statistical hypotheses," *Annals of Mathematical Statistics*, vol. 16, pp. 117–186, 1945.

[11] G. Peskir and A. Shiryaev, "Sequential testing problems for Poisson process," *Annals of Statistics*, vol. 28, pp. 837–859, 2000.

[12] H. V. Poor, *An Introduction to Signal Detection and Estimation*, second edition ed. Springer-Verlag, 1994.

[13] M. Kulldorff, R. Davis, M. Kolczak, E. Lewis, T. Lieu, and R. Pkatt, "A maximized sequential probability ratio test for drug and vaccine safety surveillance," *Sequential Analysis*, vol. 30, pp. 58–78, 2011.

[14] S. M. Brennan, A. M. Mielke, and D. C. Torney, "Radioactive source detection by sensor networks," *IEEE Transactions on Nuclear Science*, vol. 52, no. 3, pp. 813–819, 2005.

[15] D. Stephens Jr and A. Peurrung, "Detection of moving radioactive sources using sensor networks," *IEEE Transactions on Nuclear Science*, vol. 51, no. 5, pp. 2273–2278, 2004.

[16] A. Sundaresan, P. K. Varshney, and N. S. V. Rao, "Distributed detection of a nuclear radioactive source using fusion of correlated decisions," in *Proceedings of the International Conference on Information Fusion*. IEEE, 2007, pp. 1–7.

[17] A. Klimenko, W. Priedhorsky, H. Tanner, K. Borozdin, and N. Hengartner, *Intelligent Sensor Management in Nuclear Searches and Radiological Surveys*, 2006, pp. 21–22.

[18] C. D. Pahlajani, I. Poulakakis, and H. G. Tanner, "Decision making in a sensor network with Poisson process observations," in *IEEE American Control Conference*, 2013 (submitted).

[19] J. Neyman and E. S. Pearson, "On the problem of the most efficient tests of statistical hypothesis," *Philosophical Transactions of the Royal Society of London*, vol. 231, pp. 289–337, 1933.